Supporting Information

Kinetically Favorable Edge-Type Iron-Cobalt Atomic Pair Sites Synthesized via a Silica Xerogel Approach for Efficient Bifunctional Oxygen Electrocatalysis

Maosong Liu,[a] Xianhe Lv,[a] Lijuan Wang,[a] Kangmin Chen,[b] Yanxiao Li,[b] Tao Sun,[a] Jianming Zhang,[a] Long Zhang,[a]* Shuhui Sun[c]**

[a]Institute of Quantum and Sustainable Technology (IQST), School of Chemistry and Chemical Engineering, Jiangsu University, Zhenjiang, 212013, P. R. China.

[b]Instrumental Analysis Center, Jiangsu University, Zhenjiang, 212013, P. R. China

[c]Institut National de la Recherche Scientifique (INRS), Énergie Matériaux Télécommunications Research Centre, Québec J3X 1P7, Canada

Corresponding author e-mail: zhangjm@ujs.edu.cn (J.Zhang), longzhang@ujs.edu.cn (L.Zhang), shuhui.sun@inrs.ca (S.Sun)

Experimental section

Materials

Chemicals: Ferrous gluconate hydrate, sodium gluconate and glucosamine hydrochloride were purchased from Shanghai Aladdin Biochemical Technology Co. Ltd. Cobalt chloride hexahydrate ($CoCl_2·6H_2O$), ethanol, tetraethyl orthosilicate (TEOS), potassium hydroxide (KOH), hydrochloric acid (HCl) and hydrofluoric acid (HF) were purchased from Sinopharm Chemical Reagent Co. Ltd. All the chemicals were used as received without further purification. Water was purified by a Millipore water system with a resistivity of 18.2 MΩ·cm at 25 °C.

In-situ synthesis of xerogel

To 13 mL of H_2O, 0.3 g of sodium gluconate and 0.15 g of $CoCl_2·6H_2O$ were added and stirred at room temperature to prepare cobalt gluconate. Two hours later, 1.5 g of glucosamine hydrochloride and 0.15 g of ferrous gluconate hydrate were added to the above solution. After all the solids were dissolved completely, 10 mL of ethanol and 10 mL of TEOS were introduced, followed by adding 50 μL of HCl as the catalyst. This solution was stirred ceaselessly at room temperature until the formation of silica sol-gel. The sol-gel was then freeze-dried for 12 h to form dry xerogel powder.

Ex-situ synthesis of xerogel

Firstly, 10 mL of ethanol and 10 mL of TEOS were introduced to 13 mL of H_2O, followed by adding 50 μL of HCl and stirred ceaselessly at room temperature until the formation of silica sol-gel. The sol-gel was then freeze-dried for 12 h to form dry silica xerogel powder. Then, to 13 mL of H_2O, 0.3 g of sodium gluconate and 0.15 g of $CoCl_2·6H_2O$ were added and stirred at room temperature. Two hours later, 1.5 g of glucosamine hydrochloride, 0.15 g of ferrous gluconate hydrate and 5 g of silica xerogel powder were added to the above solution. This solution was stirred ceaselessly at room temperature until the formation of silica sol-gel. The sol-gel was then freeze-dried for 12 h to form dry xerogel powder.

Preparation of ISG Fe,Co-NC

Typically, 1 g of the xerogel powder (prepared by *in-situ* method) and 1 g of urea were fully grounded and mixed. The collected powder was then thermally treated at 900 ℃ for 2 h under flowing Ar (the heating rate was set to be 5 ℃/min). The black powder was etched overnight with

HF solution, followed by washing with deionized water and ethanol to remove acid residue. The etched powder was dried in vacuum for 8 h and underwent the second thermal treatment at 900 ℃ for 2 h under flowing argon (Ar) gas with a heating rate of 5 ℃/min. The sample was cooled naturally to room temperature, yielding the ISG Fe-Co-NC. The preparation of ESG Fe,Co-NC was the same as that of ISG Fe,Co-NC. The ESG Fe,Co-NC was prepared by the same condition but the xerogel powder that was prepared by *ex-situ* method was added.

Electrochemical evaluation

A three-electrode system was used for electrochemical evaluation, which was controlled by CHI760e electrochemical station (CH Instrument, USA). The working electrode was a rotating ring-disk electrode (RRDE, Pine Instrument), and the disk electrode is a glassy carbon electrode with a diameter of 4 mm. The counter electrode is platinum wire while the reference electrode is Ag/AgCl electrode in which the internal electrolyte is saturated potassium chloride solution.

The ink dripped on the electrode surface was prepared by the following method: typically, 5 mg of the catalyst sample, 500 μL of H_2O, 500 μL of ethanol and 40 μL of 5% Nafion solution were mixed together, followed by ultrasonic dispersion for more than 30 minutes to form homogeneous ink. Afterward, 10 μL of the ink was dropped on the electrode surface and left until the catalyst was evenly dispersed on the electrode surface and evaporation of ethanol and H_2O. This electrode was conducted for the electrochemical test. The cyclic voltammograms (CVs) were obtained at 0.1 M of KOH of high purity N_2 or O_2 (scan rate: 50 mV s^{-1}). All linear sweep voltammograms (LSVs) were measured in 0.1 M of KOH saturated with high purity O_2 (scan rate: 10 mV s^{-1}; rotational speed: 400-2500 rpm).

The electron transfer number (n, S1) and the yield of the intermediate (HO_2^-, S2) during the ORR process were determined from rotating ring-disk electrode measurements and calculated by the following equations:

$$n = \frac{4I_d}{\left(I_d + \frac{I_r}{N}\right)} \qquad S1$$

$$HO_2^-(\%) = \frac{200\left(\frac{I_r}{N}\right)}{I_d + \frac{I_r}{N}} \qquad S2$$

where I_d, I_r, and N denote disk current, ring current and collection efficiency of Pt ring (0.37), respectively.

All the recorded potentials were corrected to RHE using the following equation:

$$E_{RHE} = E_{Ag/AgCl} + 0.059PH + 0.197 \qquad S3$$

where E_{RHE} and $E_{Ag/AgCl}$ refer to potential relevant to reversible hydrogen electrode (RHE) and Ag/AgCl electrode, respectively.

ZAB test

Zinc-air battery tests: A home-constructed Zn-air cell was used to assess the performance of the ZAB. The electrolyte was a mixed solution of 0.2 M $ZnCl_2$ and 6 M KOH. The anode was a polished Zn plate with a 0.3 mm thickness. the gas diffusion layer (GDL) at the air cathode was created by hot-pressing carbon black onto the surface of carbon paper for 1 min at 80 °C. The catalyst ink was made by ultrasonically combining 1 mL of H_2O and 1 mL of ethanol with 10 mg as-prepared sample and 80 μL 5% Nafion solution (catalyst loading: 2 mg cm^{-2}). The achieved catalyst layer was dried in a vacuum oven under 60 ℃. The charge-discharge polarization curve was obtained by LSV test (scan rate: 10 mV s^{-1}). And the current density for the charge-discharge cycle curve test is set at 10 mA cm^{-2} and 20 mA cm^{-2}, respectively. The time of each cycle is set as 1 h (including 30 min for charging time and 30 min for discharging time).

The power density was calculated according to the equation:

$$power\ density = current\ density * voltage \qquad S4$$

The specific capacity was calculated according to the equation:

$$specific\ capacity = \frac{current * test\ hours}{consumed\ zinc\ plate\ mass} \qquad S5$$

Characterizations

The morphology of the samples was characterized using a Talos F200X transmission electron microscopy (TEM) at Thermo Fisher Nanoport Shanghai. Aberration corrected high-angle annular dark-field scanning TEM (HAADF-STEM) was conducted at Thermo Fisher Nanoport Europe (Netherland) using a Spectra 300. X-ray Photoelectron Spectroscopy (XPS) measurements were performed on ESCALAB Xi+ at Thermo Fisher Nanoport Shanghai. Raman spectra were recorded with a Thermo Fisher DXR with a laser wavelength of 532 nm. X-Ray diffraction (XRD) patterns

were collected using a Bruker D8 with the X-ray source being Cu-Kα radiation operated at 3 kV. Inductively coupled plasma optical emission spectrometer (ICP-OES) was carried out with Agilent 720ES. Synchrotron X-ray absorption spectroscopy (XAS) spectra were tested in Taiwan Light Source (Hard x-ray, 5-40K eV). Brunauer-Emmett-Teller (BET) experiments were conducted at 77 K on an AUTOSORB IQ Instrument, Quantachrome. Micro computed tomography (Micro-CT) was performed using inspeXio SMX-225CT FPD HR at Shimatsu Co. Ltd Shanghai.

Theoretical calculation

First-principles calculations were carried out using DFT with generalized gradient approximation (GGA) of Perdew-Burke-Ernzerhof (PBE) implemented in Vienna Ab-Initio Simulation Package (VASP) [1, 2]. The valence electronic states were expanded on the basis of plane waves with the core-valence interaction represented using the projector augmented plane wave (PAW) approach [3] and a cutoff of 520 eV. Convergence is achieved when the forces acting on ions become smaller than 0.02 eV/Å.

For ORR calculation, the four-electrons pathway under base condition are generally proceed in the following steps:[4]

(1) $O_2(g) + {}^* \rightarrow O_2^*$

(2) $O_2^* + H_2O(l) + e^- \rightarrow OOH^* + OH$

(3) $OOH^* + e^- \rightarrow O^* + OH$

(4) $O^* + H_2O(l) + e^- \rightarrow OH^* + OH$

(5) $OH^* + e^- \rightarrow OH^* + {}^*$

The reaction free energy (ΔG) is further calculated using the following formula:

$$\Delta G = \Delta H - T\Delta S - qU + kBTln10 \times pH$$

where ΔH is the reaction enthalpy of an elementary step and estimated by the reaction energy (ΔE) with zero-point energy (ZPE) correction from DFT calculations; $T\Delta S$ is the contribution in free energy changes from the entropy; U is the applied potential in electrode; q is the charge transfer in each step.

For calculation of OER in an alkaline condition, OER could take place in the following four-electron pathways:[4]

(1) $H_2O(l) + {}^* \leftrightarrow HO^* + H^+ + e^- \ (\Delta G_1)$

(2) $HO^* + {}^* \leftrightarrow O^* + H^+ + e^- \ (\Delta G_2)$

(3) $O^* + H_2O(l) + {}^* \leftrightarrow HOO^* + H^+ + e^- \ (\Delta G_3)$

(4) $HOO^* \leftrightarrow O_2(g) + H^+ + e^- \ (\Delta G_4)$

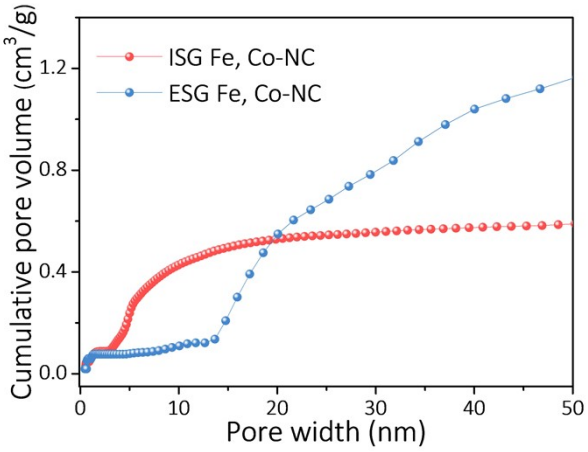

Figure S1. Cumulative pore size distribution using QSDFT model.

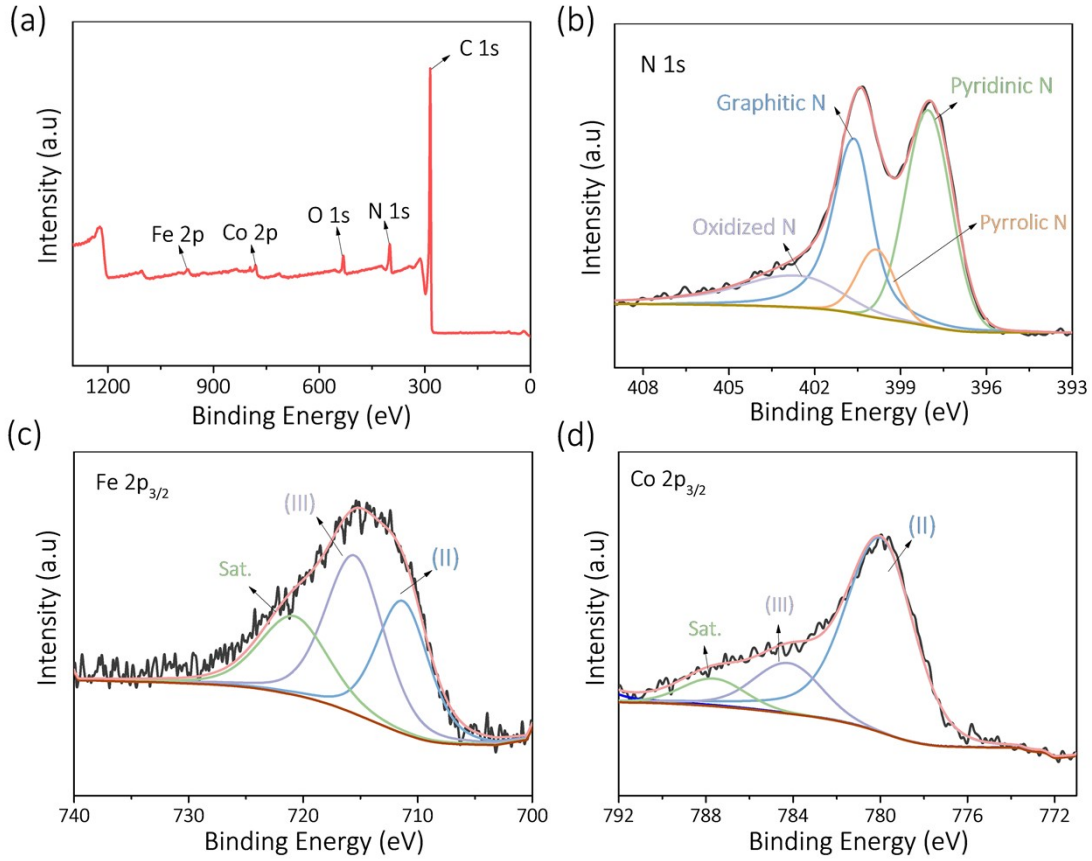

Figure S2. XPS survey spectrum (a) and high-resolution XPS spectra of N 1s (b), Fe $2p_{3/2}$ (c) and Co $2p_{3/2}$ (d) of the ISG Fe,Co-NC sample.

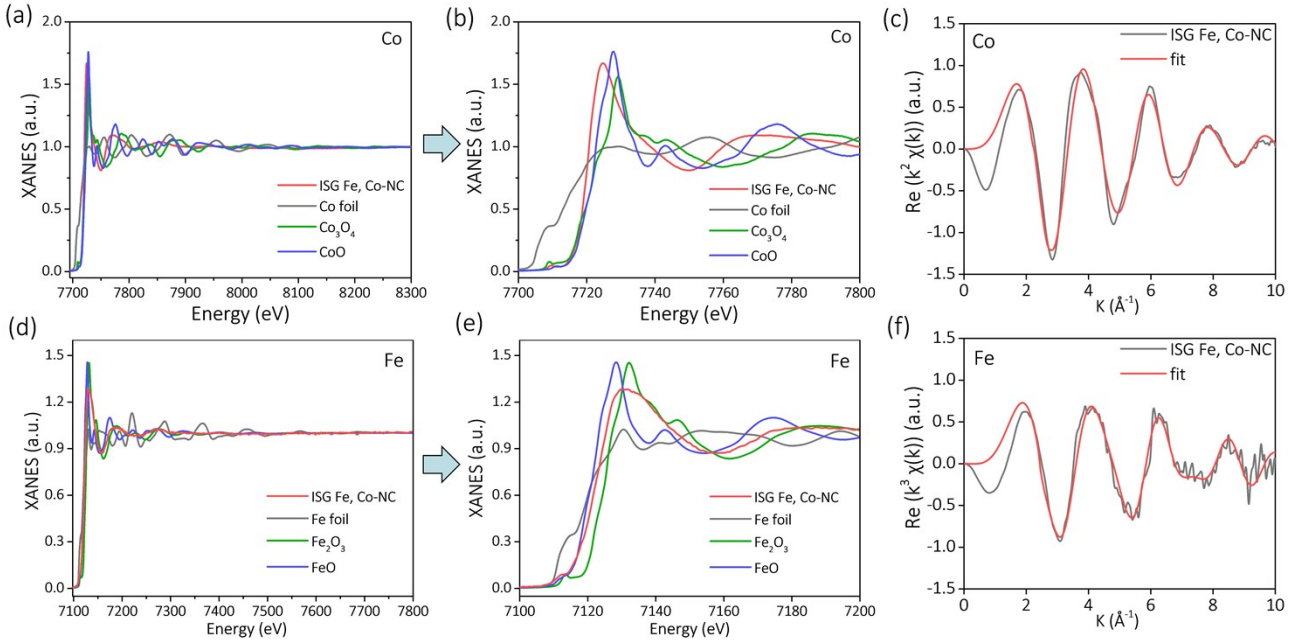

Figure S3. (a, b) Co K-edge XANES spectra of ISG Fe,Co-NC and reference samples. (c) Co EXAFS k space fitting curves of ISG Fe,Co-NC. (d, e) Fe K-edge XANES spectra of ISG Fe,Co-NC and reference samples. (f) Fe EXAFS k space fitting curves of ISG Fe,Co-NC.

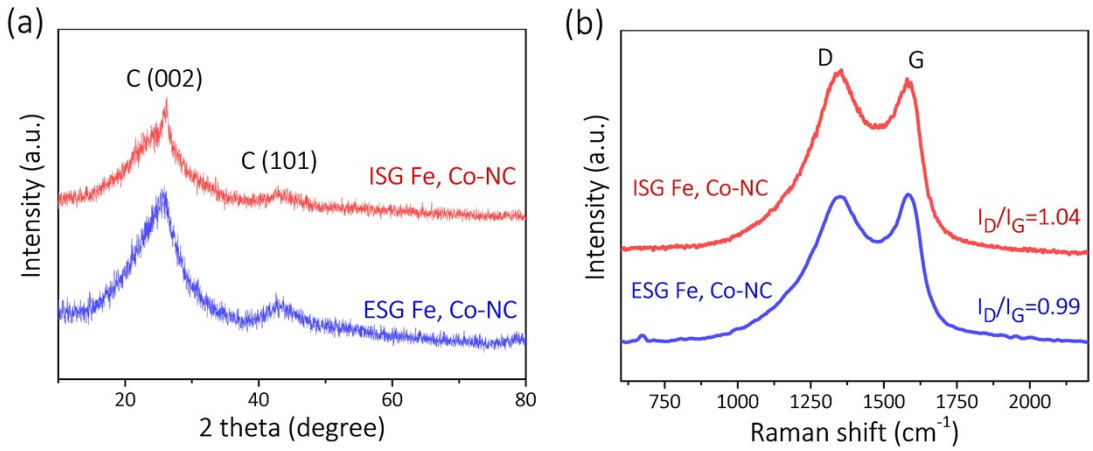

Figure S4. XRD pattern (a), Raman spectrum (b) of the ISG Fe,Co-NC and ESG Fe,Co-NC samples.

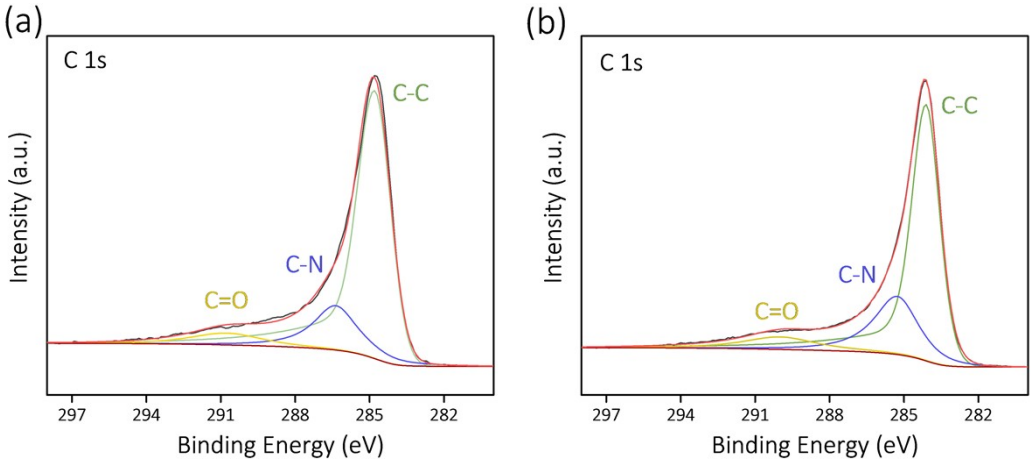

Figure S5. C 1s XPS spectra of ESG Fe,Co-NC and ISG Fe,Co-NC.

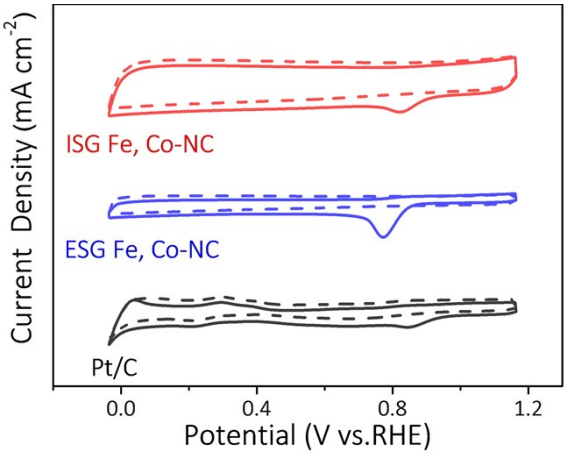

Figure S6. CV curves of ISG Fe,Co-NC, ESG Fe,Co-NC and Pt/C catalysts in O_2-saturated 0.1 M KOH.

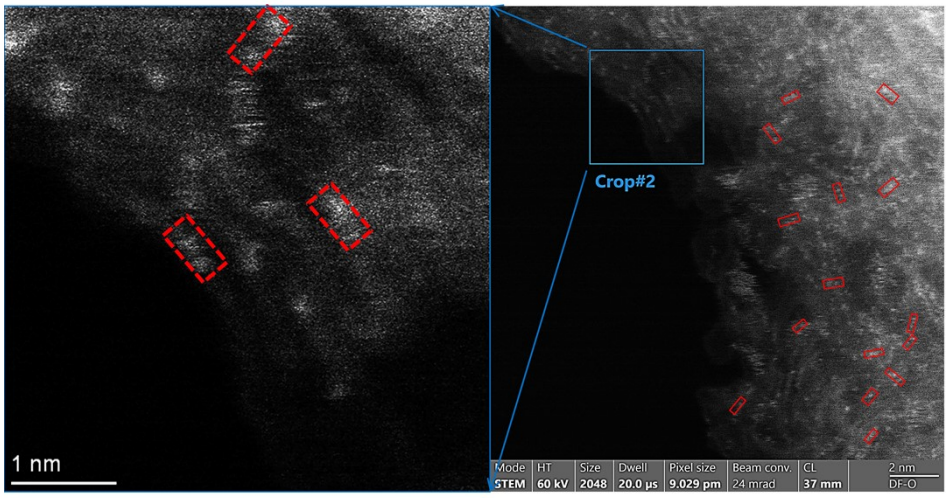

Figure S7. HAADF-STEM images of the ISG Fe,Co-NC sample after the cycling (The circles are guides for the eye, marking the possible Fe-Co atom pairs).

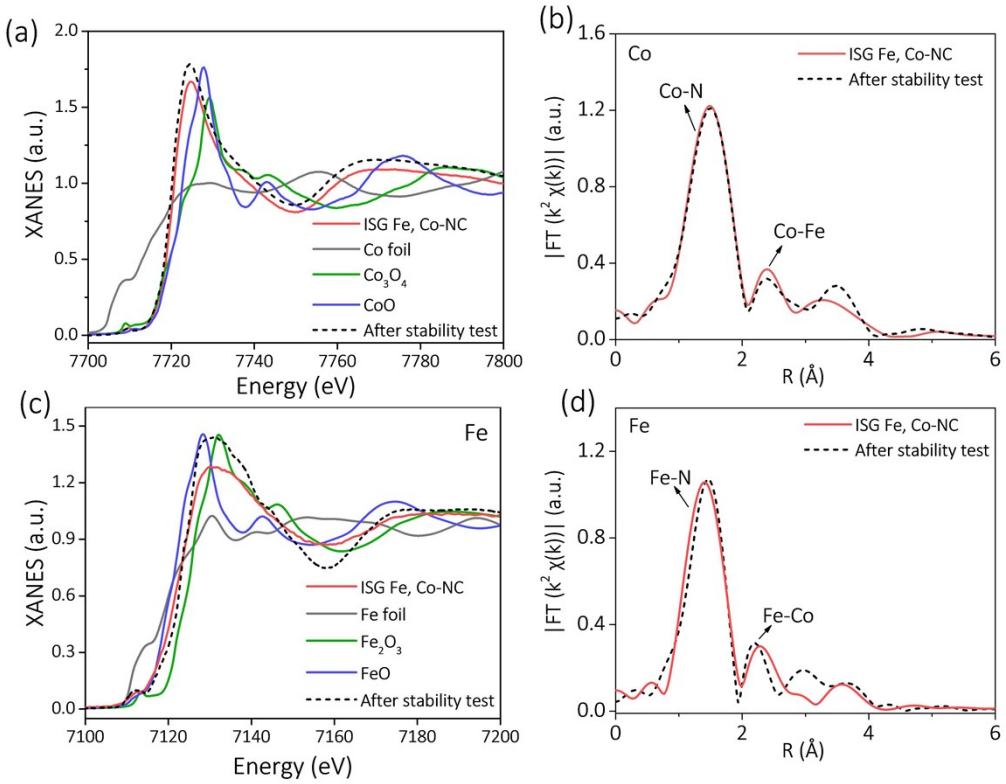

Figure S8. (a) Co K-edge XANES and (b) Fourier-transformed EXAFS spectra comparison before and after the cycling of ISG Fe,Co-NC and reference. (c) Fe K-edge XANES and (d) Fourier-transformed EXAFS spectra comparison before and after the cycling of ISG Fe,Co-NC and reference.

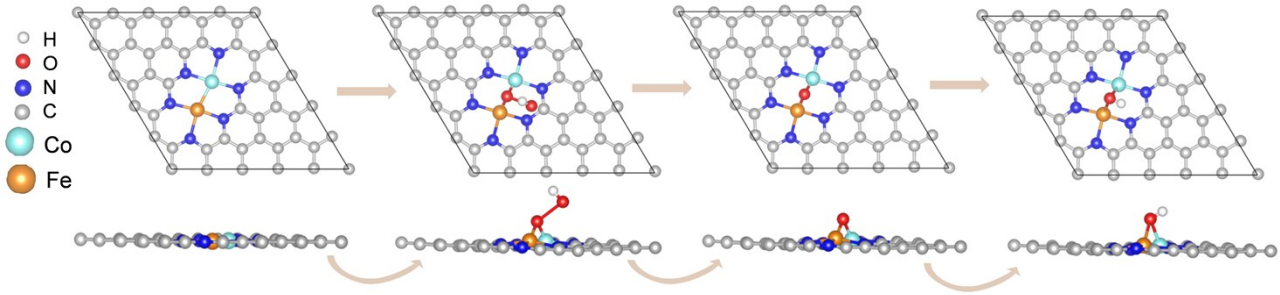

Figure S9. Top view and side view of the initial structures after adsorption of OOH*, O*, and OH* on the in-plane-type $FeCoN_6$ model. In particular, the orange, light blue, gray, dark blue, red, and white balls represent Fe-Co, C, N, O, and H atoms, respectively.

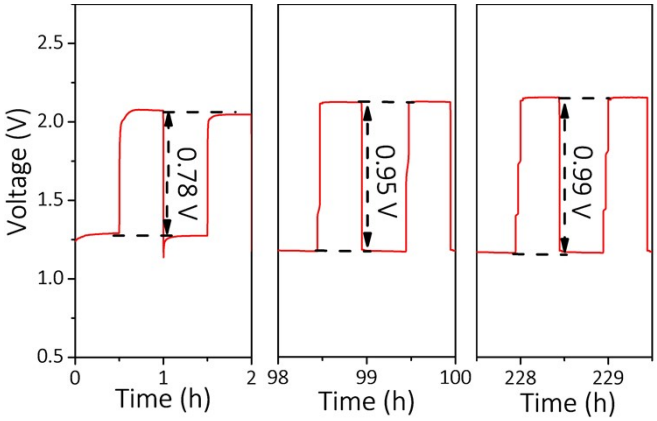

Figure S10. Long-term cycling performance of the ZAB with ISG Fe,Co-NC at a current density of 10 mA cm^{-2}.

Table S1. The surface areas for the specific distribution of pores of ISG Fe,Co-NC and ESG Fe,Co-NC.

Sample	ISG Fe,Co-NC		ESG Fe,Co-NC	
QSDFT* analysis	Surface area ($m^2\ g^{-1}$)	Pore volume ($cm^3\ g^{-1}$)	Surface area ($m^2\ g^{-1}$)	Pore volume ($cm^3\ g^{-1}$)
< 2 nm	329.41	0.136	220.28	0.077
2 - 10 nm	447.58	0.615	13.06	0.033
> 10 nm	11.74	0.207	149.83	1.056
Total	788.73	0.822	383.17	1.166

QSDFT* means quenched solid density functional theory (QSDFT) analysis.

$m^2\ g^{-1}$ means the surface area ($m^2\ g^{-1}$).

$cm^3\ g^{-1}$ means pore volume ($cm^3\ g^{-1}$).

Table S2. Mass fraction content of Co and Fe of ISG Fe,Co-NC and ESG Fe,Co-NC from ICP-OES measurements.

Catalysts	**Co content (measured by ICP, wt%)**	**Fe content (measured by ICP, wt%)**
ISG Fe,Co-NC	2.25	0.62
ESG Fe,Co-NC	0.98	0.32

Table S3. EXAFS data fitting results of the ISG Fe,Co-NC.

edge	**Path**	**N**	**R(Å)**	**σ^2*10^{-3} ($Å^2$)**	**ΔE_0 (eV)**	**R-factor**
Fe	Fe-N	3.63	1.83	9.56	-3.87	0.0058
	Fe-Co	0.60	2.59	3.32	-0.38	
Co	Co-N	3.51	1.83	5.95	-3.02	0.011
	Co-Fe	0.48	2.46	1.02	-0.15	

N is the coordination number; R is the interatomic distance (the bond length between Fe/Co atom and surrounding coordinated N atoms); ΔE_0 (eV), inner potential correction accounts for the difference in the inner potential between the sample and the reference compound. σ^2 is Debye-Waller factor value; R factor indicates the goodness of the fit.

Table S4. XPS results analysis of high-resolution C 1s spectrum for the prepared samples.

Sample	C-C (%)	C-N (%)	C=O (%)
ISG Fe,Co-NC	76.05	17.34	6.61
ESG Fe,Co-NC	67.94	23.87	8.19

Table S5. The comparison of essential parameters for evaluating bifunctional electrocatalytic activity for OER and ORR.

Catalyst	$E_{1/2}$	$E_{j=10}$	ΔE/V (vs. RHE)	Reference
ISG Fe,Co-NC	0.865	1.613	0.748	This work
ESG Fe,Co-NC	0.798	1.747	0.948	
Pt/C	0.851	/	0.776	
IrO_2	/	1.629		
Fe-NC/Co-NC mixture	0.849	1.703	0.854	
meso/micro-FeCo-N_x-CN-30	0.886	1.67	0.78	[5]
CoNi-SAs/NC	0.76	1.57	0.81	[6]
$Ni_{66}Fe_{34}$-NC	0.85	1.697	0.847	[7]
Co SA@NCF/CNF	0.88	1.63	0.75	[8]
Fe-N_x-C	0.91	1.83	0.92	[9]
Co-NC@LDH	0.8	1.619	0.819	[10]
CoSAs@CNTs	0.86	1.64	0.78	[11]
Co_xNi-N/C	0.84	1.59	0.78	[12]
Co-POC	0.83	1.70	0.87	[13]
Fe–N_4 SAs/NPC	0.885	1.66	0.775	[14]

Table S6. The comparison of essential parameters for ISG Fe,Co-NC and ISG Fe-NC/Co-NC

Catalyst	Metal content (measured by ICP, wt %)	Mainly mesopore size (nm)	BET surface area ($m^2 g^{-1}$)
ISG Fe,Co-NC	Fe (0.62), Co (2.25)	5 ~ 6	778.73
ISG Fe-NC/Co-NC mixture	Fe (0.65), Co (2.28)	4 ~ 6	791.53

Table S7. Gibbs adsorption free energy for adsorbates of edge-type Fe,Co-NC and in-plane-type Fe,Co-NC at different potentials for ORR.

G_{ads} (eV)	U = 0 V		U = 1.23 V	
	edge-type Fe,Co-NC	in-plane-type Fe,Co-NC	edge-type Fe,Co-NC	in-plane-type Fe,Co-NC
O_2(g)	4.92	4.92	0	0
***OOH**	4.177	4.723	0.487	1.033
***O**	2.98	3.304	0.52	0.844
***OH**	1.581	1.821	0.351	0.591
H_2O	0	0	0	0

Table S8. Gibbs free energy change (ΔG) of edge-type Fe,Co-NC and in-plane-type Fe,Co-NC at different potentials for ORR.

ΔG_{ads} (eV)	U = 0 V		U = 1.23 V	
	edge-type Fe,Co-NC	in-plane-type Fe,Co-NC	edge-type Fe,Co-NC	in-plane-type Fe,Co-NC
Step1	-0.743	-0.197	0.487	1.033
Step2	-1.197	-1.419	0.033	-0.189
Step3	-1.399	-1.483	-0.169	-0.253
Step4	-1.581	-1.821	-0.351	-0.591

Table S9. Gibbs adsorption free energy for adsorbates of edge-type Fe,Co-NC and in-plane-type Fe,Co-NC at different potentials for OER.

ΔG_{ads} (eV)	U = 0 V		U = 1.23 V	
	edge-type Fe,Co-NC	in-plane-type Fe,Co-NC	edge-type Fe,Co-NC	in-plane-type Fe,Co-NC
O_2(g)	0	0	0	0
***OOH**	1.581	1.821	0.351	0.591
***O**	2.98	3.304	0.52	0.844
***OH**	4.177	4.723	0.487	1.033
H_2O	4.92	4.92	0	0

Table S10. Gibbs free energy change (ΔG) of edge-type Fe,Co-NC and in-plane-type Fe,Co-NC at different potentials for OER.

ΔG_{ads} (eV)	U = 0 V		U = 1.23 V	
	edge-type Fe,Co-NC	in-plane-type Fe,Co-NC	edge-type Fe,Co-NC	in-plane-type Fe,Co-NC
Step1	1.581	1.821	0.351	0.591
Step2	1.399	1.483	0.169	0.253
Step3	1.197	1.419	-0.033	0.189
Step4	0.743	0.197	-0.487	-1.033

References

1. J. P. Perdew, K. Burke and M. Ernzerhof, *Phys. Rev. Lett.*, 1996, **77**, 3865-3868.
2. G. Kresse and J. Furthmüller, *Phys. Rev. B*, 1996, **54**, 11169-11186.
3. P. E. Blöchl, *Phys. Rev. B*, 1994, **50**, 17953-17979.
4. J. K. Nørskov, J. Rossmeisl, A. Logadottir, L. Lindqvist, J. R. Kitchin, T. Bligaard and H. Jónsson, *J. Phys. Chem. B*, 2004, **108**, 17886-17892.
5. S. Li, C. Cheng, X. Zhao, J. Schmidt and A. Thomas, *Angew. Chem. Int. Ed.,* 2018, **57**, 1856-1862.
6. X. Han, X. Ling, D. Yu, D. Xie, L. Li, S. Peng, C. Zhong, N. Zhao, Y. Deng and W. Hu, *Adv. Mater.*, 2019, **31**, 1905622.
7. M. Ma, A. Kumar, D. Wang, Y. Wang, Y. Jia, Y. Zhang, G. Zhang, Z. Yan and X. Sun, *Appl. Catal. B*, 2020, **274**, 119091.
8. D. Ji, L. Fan, L. Li, S. Peng, D. Yu, J. Song, S. Ramakrishna and S. Guo, 2019, *Adv. Mater.*, **31**, 1808267.
9. J. Han, X. Meng, L. Lu, J. Bian, Z. Li and C. Sun, *Adv. Funct. Mater.*, 2019, **29**, 1808872.
10. D. Chen, X. Chen, Z. Cui, G. Li, B. Han, Q. Zhang, J. Sui, H. Dong, J. Yu, L. Yu and L. Dong, *Chem. Eng. J.*, 2020, **399**, 125718.
11. S. Dilpazir, H. He, Z. Li, M. Wang, P. Lu, R. Liu, Z. Xie, D. Gao and G. Zhang, *ACS Appl. Energy Mater.*, 2018, **1**, 3283-3291.
12. Z. Li, H. He, H. Cao, S. Sun, W. Diao, D. Gao, P. Lu, S. Zhang, Z. Guo, M. Li, R. Liu, D. Ren, C. Liu, Y. Zhang, Z. Yang, J. Jiang and G. Zhang, *Appl. Catal. B,* 2019, **240**, 112-121.
13. B.-Q. Li, C.-X. Zhao, S. Chen, J.-N. Liu, X. Chen, L. Song and Q. Zhang, *Adv. Mater.*, 2019, **31**, 1900592.
14. Y. Pan, S. Liu, K. Sun, X. Chen, B. Wang, K. Wu, X. Cao, W.-C. Cheong, R. Shen, A. Han, Z. Chen, L. Zheng, J. Luo, Y. Lin, Y. Liu, D. Wang, Q. Peng, Q. Zhang, C. Chen and Y. Li, *Angew. Chem. Int. Ed.*, 2018, **57**, 8614-8618.